J|A|C|S
ARTICLES
Published on Web 03/03/2007

Synthesis and Mechanistic Study of Palladium Nanobars and Nanorods

Yujie Xiong,[†] Honggang Cai,[†] Benjamin J. Wiley,[‡] Jinguo Wang,[§] Moon J. Kim,[§] and Younan Xia*,[†]

Contribution from the Department of Chemistry, and Department of Chemical Engineering, University of Washington, Seattle, Washington 98195, and Department of Electrical Engineering, University of Texas at Dallas, Richardson, Texas 75083

Received December 8, 2006; E-mail: xia@chem.washington.edu

Abstract: This paper describes a simple and versatile method for growing highly anisotropic nanostructures of Pd, single-crystal nanobars bounded by {100} facets and single-crystal nanorods with their side surfaces enclosed by {100} and {110} facets. According to thermodynamic arguments, Pd atoms should nucleate and grow in a solution phase to form cuboctahedrons of spherical shape with their surfaces bounded by a mix of {111} and {100} facets. Anisotropic nanostructures can only form under kinetically controlled conditions, while the cubic symmetry is broken. In the present system, we found that one-dimensional growth could be induced and maintained through an interplay of the following processes: (i) speedy reduction of the precursor to ensure prompt addition of atoms to the seed; (ii) chemisorption of bromide on the seed to promote the formation of {100} and {110} facets; and (iii) localized oxidative etching on one specific face of the seed to initiate preferential growth on this face. Experimentally, the anisotropic growth can be achieved by varying the type and concentration of reducing agent, as well as by adjusting the reaction temperature. This methodology developed for Pd has also been extended to both Au and Pt. As expected for a kinetically controlled product, the anisotropic nanostructure evolved into the thermodynamically favored shape during an aging process.

1. Introduction

Single-crystal, one-dimensional (1-D) nanostructures of Pd are attractive as interconnects for fabricating nanoscale electronic devices. For example, Pd can form reliable and reproducible ohmic contacts with carbon nanotubes (CNTs) because Pd has a relatively high work function and can easily wet the carbon surface. This capability allows one to elucidate the intrinsic properties of CNTs and to maximize the performance of CNT-based devices such as field-effect transistors (FETs).[1] Another important property of Pd is its exceptional sensitivity toward hydrogen. To this end, polycrystalline, mesoscopic wires made of Pd have been utilized for resistance-based detection of hydrogen gas.[2] However, polycrystalline wires containing gaps between adjacent grains often shrink after initial exposure to hydrogen and may cause random, irreversible changes to the resistance of a sensing device. It should be possible to overcome this problem by switching to single-crystalline Pd nanowires with better controlled characteristics.

One of the simplest ways to generate 1-D nanostructures of metals is to confine their growth within a template. The nanoscale channels in alumina or polycarbonate membranes have been most commonly used for this purpose.[3] Other types of templates include mesoporous silica,[4] cylindrical micelles,[5] and organic block copolymers,[6] as well as the edges or grooves on solid substrates.[7] Although a template-directed synthesis can be very simple and straightforward, it is limited in terms of the quantity of nanostructures that can be produced in each run of synthesis. It often yields polycrystalline nanostructures, which are less valuable for both fundamental study and device fabrication. In addition, the template needs to be removed in a postsynthesis step so the metal nanostructures can be harvested and put to use. As a result, it seems to be impractical to rely on template-directed synthesis if one needs single-crystal, 1-D nanostructures of Pd.

Solution-phase growth has received considerable interest for its capability to produce single-crystal nanostructures with high quality. However, it is not easy to grow 1-D nanostructures of

[†] Department of Chemistry, University of Washington.
[‡] Department of Chemical Engineering, University of Washington.
[§] University of Texas at Dallas.

(1) (a) Javey, A.; Guo, J.; Wang, Q.; Lundstrom, M.; Dai, H. *Nature* **2003**, *424*, 654. (b) Mann, D.; Javey, A.; Kong, J.; Wang, Q.; Dai, H. *Nano Lett.* **2003**, *3*, 1541. (c) Zhu, W.; Kaxiras, E. *Nano Lett.* **2006**, *6*, 1415.
(2) Favier, F.; Walter, E. C.; Zach, M. P.; Benter, T.; Penner, R. M. *Science* **2001**, *293*, 2227.
(3) (a) Martin, C. R. *Science* **1994**, *266*, 1961. (b) Martin, B. R.; Dermody, C. J.; Reiss, B. D.; Fang, M.; Lyon, L. A.; Natan, M. J.; Mallouk, T. E. *Adv. Mater.* **1999**, *11*, 1021.
(4) (a) Huang, M. H.; Choudrey, A.; Yang, P. *Chem. Commun.* **2000**, 1063. (b) Han, Y.; Kim, J.; Stucky, G. D. *Chem. Mater.* **2000**, *12*, 2068. (c) Lee, K.-B.; Lee, S.-M.; Cheon, J. *Adv. Mater.* **2001**, *294*, 348.
(5) Kijima, T.; Yoshimura, T.; Uota, M.; Ikeda, T.; Fujikawa, D.; Mouri, S.; Uoyama, S. *Angew. Chem., Int. Ed.* **2004**, *43*, 228.
(6) Cornelissen, J. J. L. M.; Van Heerbeek, R.; Kamer, P. C. J.; Reek, J. N. H.; Sommerdijk, N. A. M.; Nolte, R. J. M. *Adv. Mater.* **2002**, *14*, 489.
(7) (a) Bishop, D. J.; Licini, J. C.; Dolan, G. J. *Appl. Phys. Lett.* **1985**, *46*, 1000. (b) Jones, E. T. T.; Chyan, O. M.; Wrighton, M. S. *J. Am. Chem. Soc.* **1987**, *109*, 5526. (c) Penner, R. M. *J. Phys. Chem. B.* **2002**, *106*, 3339.

10.1021/ja0688023 CCC: $37.00

Pd in a solution phase. As a face-centered cubic (*fcc*) metal, Pd has no intrinsic driving force for the growth of anisotropic structures when the seeds are surrounded by an isotropic medium. As dictated by thermodynamics, Pd atoms are expected to nucleate and grow into cuboctahedrons (with a nearly spherical shape) enclosed by a mix of {111} and {100} facets to minimize the total surface energy.[8] This prediction has recently been verified by experimental studies where 8-nm cuboctahedrons were obtained as the major product when a Pd precursor was reduced at a sufficiently fast rate to exclude any kinetic effect.[9] In general, an *fcc* metal can only be forced to grow into anisotropic nanostructures through the kinetic control. As demonstrated in our previous work, triangular and hexagonal thin plates of Pd could be prepared by operating at an extremely slow reduction rate to induce the formation of stacking faults and thus break the cubic symmetry. For such thin plates, the top and bottom faces account for >70% of the surface and are terminated in {111} facets, while the side faces (<30% of the surface) are enclosed by {100} and {111} facets.[10] It is evident that one needs to not only break the cubic symmetry but also substantially increase the coverage of {100} and/or {110} facets on the surface to generate nanostructures with 1-D morphology.[11]

Here, we demonstrate that the formation of {100} and {110} facets can be greatly promoted by introducing bromide into the reaction solution. The bromide is able to chemisorb onto the surface of Pd seeds and alter the order of surface free energies for different facets. By fine-tuning the experiment conditions, we can selectively generate nanobars, structures with a square cross-section and enclosed by {100} facets, and nanorods, structures with an octagonal cross-section whose side surface is bounded by a mix of {100} and {110} facets. Systematic studies suggest that the anisotropic growth is most likely induced by localized oxidative etching on one specific face of a seed, which creates an active site for atomic addition (i.e., growth) and thus facilitates the preferential growth on this face. When the rate of atomic addition is sufficiently fast, the preferential growth on this particular face leads to the formation of an elongated nanostructure with a square cross-section. More specifically, when the reduction rate is in the medium region, the seeds take a cubic shape with slight truncation at the corners, and the product mainly contains nanobars. As the reduction rate becomes much faster, more seeds are formed in the nucleation step. These cubic seeds take a smaller size but with more significant truncation at the corners, and the final product is dominated by nanorods thinner than the nanobars. Because the nanobars and nanorods are kinetically controlled products, they can be aged and transformed into cuboctahedrons, a shape more favorable from the viewpoint of thermodynamics. This approach developed for Pd can also be applied to both Au and Pt.

(8) (a) Wulff, G. *Z. Kristallogr.* **1901**, *34*, 449. (b) Marks, L. D. *Rep. Prog. Phys.* **1994**, *57*, 603. (c) Pimpinelli, A.; Villain J. *Physics of Crystal Growth*; Cambridge University Press: Cambridge, UK, 1998.
(9) Xiong, Y.; Chen, J.; Wiley, B.; Xia, Y.; Aloni, S.; Yin, Y. *J. Am. Chem. Soc.* **2005**, *127*, 7332.
(10) Xiong, Y.; McLellan, J. M.; Chen, J.; Yin, Y.; Li, Z.-Y.; Xia, Y. *J. Am. Chem. Soc.* **2005**, *127*, 17118.
(11) (a) Wang, Z. L.; Mohamed, M. B.; Link, S.; El-Sayed, M. A. *Surf. Sci.* **1999**, *440*, L809. (b) Wang, Z. L. *J. Phys. Chem. B* **2000**, *104*, 1153. (c) Wang, Z. L.; Gao, R. P.; Nikoobakht, B.; El-Sayed, M. A. *J. Phys. Chem. B* **2000**, *104*, 5417.

2. Experimental Section

Chemicals and Materials. Ethylene glycol (EG, J. T. Baker, 9300-01), sodium palladium(II) chloride (Na_2PdCl_4, Aldrich, 379808-1g), potassium bromide (KBr, Fisher, P205-100g), and poly(vinyl pyrrolidone) (PVP, MW = 55 000, Aldrich, 856568-100g) were all used as received without further purification.

Synthesis of Pd Nanorods with an Aspect Ratio of 8. In a typical synthesis, 5 mL of EG was hosted in a 25-mL, three-neck flask (equipped with a reflux condenser and a Teflon-coated magnetic stirring bar) and heated in air under magnetic stirring at 100 °C. Meanwhile, 0.0486 g of Na_2PdCl_4 and 0.600 g of KBr were dissolved in 3 mL of water, and 0.0916 g of PVP was dissolved in 3 mL of EG at room temperature. These two solutions (with the molar ratio of $PdCl_4^{2-}$ to Br^- and the repeating unit of PVP being 1:30:15) were then injected simultaneously into the flask using a two-channel syringe pump (KDS-200, Stoelting, Wood Dale, IL) at a rate of 45 mL per hour. The reaction mixture was heated at 100 °C in air for 1 h before the product was collected by centrifugation and washed with acetone once and with ethanol three times to remove most of the EG and excess PVP. The as-obtained samples were characterized by transmission electron microscopy (TEM), high-resolution TEM, electron diffraction (ED), energy-dispersive X-ray (EDX) analysis, powder X-ray diffraction (PXRD), and X-ray photoelectron spectroscopy (XPS).

Synthesis of Pd Nanobars with Aspect Ratios of 2−4. The procedure was similar to what was used for the Pd nanorods, except that the PVP was dissolved in 3 mL of water instead of EG.

Synthesis of Pd Nanobars with Aspect Ratios of 1−1.2. The procedure was similar to the one used for the Pd nanorods, except that the solvent for all solutions was water instead of EG. In this case, the hydroxyl end group of PVP served as the reducing agent.

Instrumentation. TEM images were captured using a Phillips 420 transmission electron microscope operated at 120 kV. High-resolution TEM images and ED patterns were taken on a JEOL field-emission transmission electron microscope (2100F) operated at 200 kV. Filtered images were generated by inverse FFT with a Gatan Digital Micrograph program. EDX analysis was performed on a FEI field-emission scanning electron microscope (Sirion XL) operated at an accelerating voltage of 10 kV. Samples for TEM and EDX studies were prepared by drying a drop of the aqueous suspension of particles on carbon-coated copper grids (Ted Pella, Redding, CA) or silicon wafers under ambient conditions. Before imaging, the TEM and SEM samples were placed in a homemade, gravity-fed flow cell and washed for 1 h with deionized water to remove excess PVP. Finally, the samples were dried and stored in vacuum for TEM and EDX characterization. All powder XRD patterns were recorded using a Philips 1820 diffractometer equipped with a Cu Kα radiation source ($\lambda = 1.54180$ Å), and the samples were deposited onto glass slides.

XPS measurements were performed using a Surface Science X-Probe spectrometer equipped with an Al Kα monochromatized X-ray source ($E = 1486.6$ eV) with a penetration depth of 6−10 nm. The instrument was operated at a pressure of 5×10^{-9} Torr in the analysis chamber. The X-ray spot had an elliptical shape with a short axis of 800 μm when focused on the surface, and the analyzer had an angle of 55° with respect to the surface normal of the sample. Photoelectrons were collected with a pass energy of 150 eV for surveys and 50 eV for high-resolution spectra. The binding energies were calculated relative to the maximum intensity of the C 1s signal at 285.0 eV. Analysis of the spectra was executed using the ESCA VB data reduction software provided by Service Physics. A submonolayer of Pd nanobars was deposited on small pieces of silicon (0.5×0.5 cm^2 in size) for all XPS samples.

3. Results and Discussion

Correlation between Shape and Reduction Kinetics. We first conducted the synthesis in solutions that contained KBr,

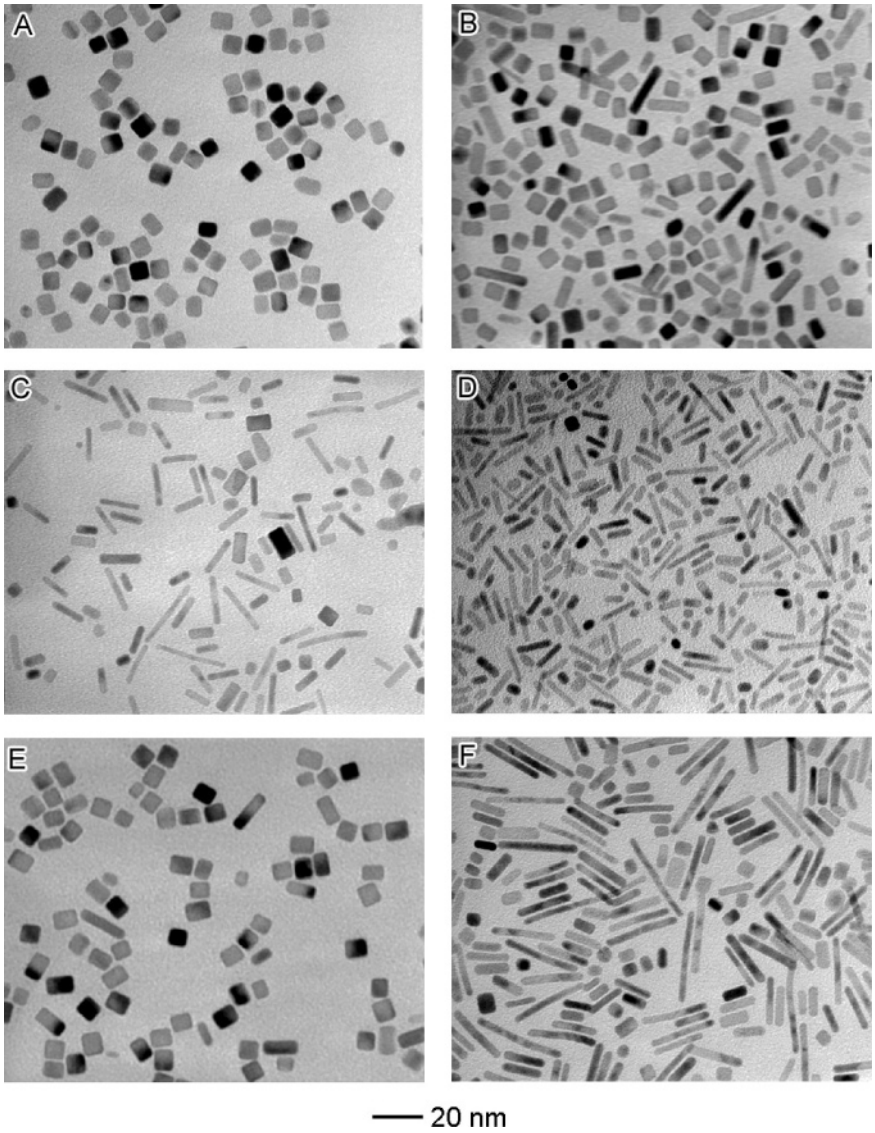

Figure 1. TEM images of Pd nanostructures that were obtained when the reduction kinetics was controlled by adjusting the volume percent of ethylene glycol (EG) in the solvent mixture: (A) 0%; (B) 9.1%; (C) 45.5%; and (D) 72.7%. The reaction temperature was 100 °C. The product shown in (E) was obtained under the same condition as in (D), except for the use of di(ethylene glycol) (DEG) instead of EG. The product shown in (F) was obtained under the same condition as in (D), except that the temperature was increased to 120 °C. All of these syntheses were carried out with a fixed molar ratio of KBr to Na_2PdCl_4 at 30, in the presence of 75 mM PVP, and in an 11-mL mixture of EG (or DEG) and water.

PVP, and different amounts of EG in water, with the addition of Na_2PdCl_4 as a precursor to Pd atoms. The key reaction involved in such a synthesis is the co-reduction of Na_2PdCl_4 by both EG and PVP. We have recently demonstrated that the ends of commercially available PVP are terminated in the hydroxyl group, which can serve as a mild reducing agent for the generation of metal nanoparticles.[12] In contrast to the weak reducing strength of PVP, EG has proven to be a more powerful reducing agent for the reduction of a metal salt.[9,10] Therefore, in the current work, the reduction rate should increase as the percent of EG in the solvent mixture is increased. Through this kinetic control, the reaction can generate a number of well-defined nanostructures, nanobars and nanorods with different aspect ratios (RAs). Figure 1A−D shows TEM images of four representative samples, illustrating the dependence of the shape of Pd nanostructures on the concentration of EG. It is clear that a faster reduction rate at a higher EG concentration induced anisotropic growth for the nanocrystals. More specifically, slow, medium, and fast reduction rates favored the formation of Pd nanobars (width, ∼8 nm; RA, 1−1.2), nanobars (width, ∼6 nm; RA, 2−4), and nanorods (diameter, ∼2 nm; RA, ∼8), respectively.[13] For nanobars and nanorods, the yield was typically >95% in each run of synthesis (see Figure 1A and D).[13] This strong dependence implies that the shape of product can be effectively altered by manipulating the reduction rate. This point is further supported by the result of a synthesis where di(ethylene glycol) (DEG) instead of EG was used as the reductant. As compared to EG, DEG has a weaker reducing power[14] and therefore shows a slower reduction rate for the Pd precursor. As a result, the reaction yielded short nanobars instead of nanorods (see Figure 1E). In addition to the change of reducing

(12) Xiong, Y.; Washio, I.; Chen, J.; Cai, H.; Li, Z.-Y.; Xia, Y. *Langmuir* **2006**, *22*, 8563.

(13) A minimum of 100 particles were used to measure lengths and widths. The values listed are averages; standard deviations in lengths are at most 20%, and standard deviations in widths are at most 10%. The yield in this paper means the fraction of all observed particles that are of a certain shape.

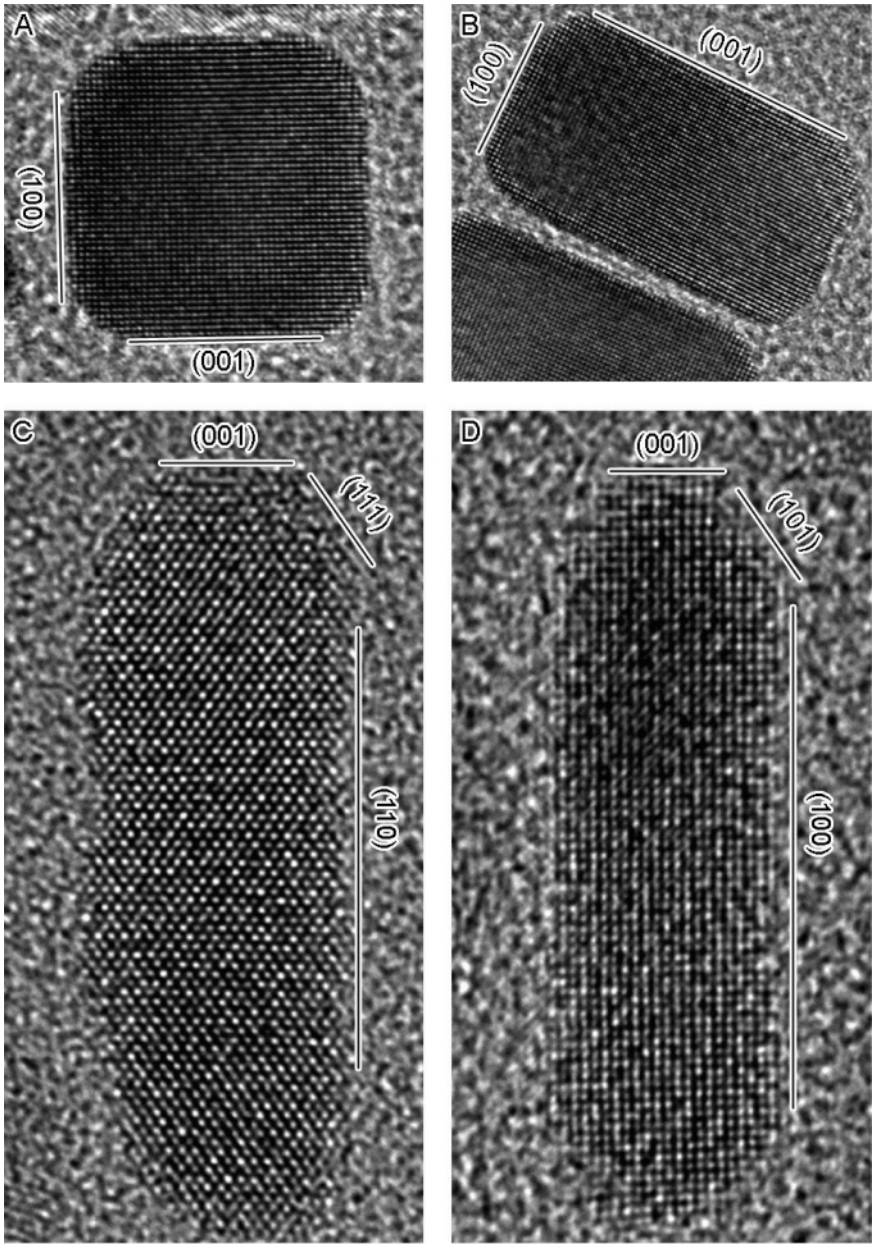

Figure 2. High-resolution TEM images of the Pd nanobars and nanorods shown in Figure 1A, B, and F: (A) a nanobar with an aspect ratio of ~1 recorded along [010]; (B) a nanobar with an aspect ratio of ~2 recorded along [010]; (C) a nanorod recorded along [1$\bar{1}$0]; and (D) a nanorod recorded along [010].

agent, the reduction kinetics can also be manipulated by adjusting reaction temperature. To this end, we found that the reduction could be accelerated to induce anisotropic growth by increasing the temperature from 100 to 120 °C while other parameters were kept the same as in Figure 1D. This increase in temperature doubled the aspect ratio of Pd nanorods from 8 to 16 while the diameter remained at 2 nm (see Figure 1F).

The structures of nanobars and nanorods were characterized by high-resolution TEM studies, as detailed in Figure 2 and Figure S1. Figure 2A shows a high-resolution TEM image of a nanobar with an aspect ratio of about 1. The fringes show a period of 2.0 Å, which was consistent with the {200} lattice spacing of *fcc* Pd. This image also displayed well-resolved, continuous fringes with the same orientation, implying that the Pd nanocube is a piece of single crystal bounded by {100} facets. Similarly, the Pd nanobar with a higher aspect ratio is also a single crystal enclosed by {100} facets, except that its dimension along one direction is much larger than those along the other two directions (see Figure 2B). All of them were slightly truncated at the corners. Different from the nanobar, the nanorod has an octagonal cross-section and its side surface is bounded by a mix of both {100} and {110} facets. It can lie on a flat surface against any one of these facets. Figure 2C shows a high-resolution TEM image of a Pd nanorod recorded along [1$\bar{1}$0], suggesting that the nanorod is a single crystal without any dislocation, stacking fault, or twin defects. This nanorod grew along the [001] direction and was supported on the TEM grid against one of its {110} facets. The ends of this nanorod were enclosed by the (001) face and {111} facets. Figure 2D

(14) (a) *Glycols*; Curme, G. O., Jr., Johnston, F., Eds.; Reinhold Publishing Co.: New York, 1952. (b) Fievet, F.; Lagier, J. P.; Figlarz, M. *MRS Bull.* **1989**, *14*, 29. (c) Bandwar, R. P.; Rao, C. P. *Carbohydr. Res.* **1995**, *277*, 197. (d) Yamaguchit, T.; Kitajima, K. *J. Mater. Sci.* **1998**, *33*, 653. (e) Teranishi, T.; Hosoe, M.; Tanaka, T.; Miyake, M. *J. Phys. Chem. B* **1999**, *103*, 3818.

shows a high-resolution TEM image of a nanorod that lies on the TEM grid against the (010) face. The ends of this nanorod were enclosed by the (001) face and {110} facets of relatively small in area. These results are similar to the experimental observations on single-crystal Au nanorods.[11] We also observed surface reconstruction for the less stable {110} facets, which has a higher surface energy relative to the {100} and {111} facets. In some regions, rows of atoms are missing along the [1$\bar{1}$0] axis, and the {110} surface was transformed into strips of {111} facets. It is known that the {111} surface has a most closely packed structure, and thus the lowest surface energy. Through this surface reconstruction, the {110} facets were stabilized on the Pd nanorods. A similar surface reconstruction has also been observed for single-crystal Au nanorods.[11c] In addition to the high-resolution TEM, the nanorods and nanobars can also be easily distinguished by the sharpness of their ends, with bars, in general, sharper than rods.

The phase purity and high crystallinity of the Pd nanostructures are also supported by powder X-ray diffraction (XRD). Figure S2 shows the typical PXRD pattern of an as-prepared sample of Pd nanobars. In the XRD pattern, all of the peaks can be indexed to *fcc* palladium (JCPDS card, 05-0681). No characteristic peaks were observed for impurities such as $PdBr_2$ and PdO. The ratio between the intensities of (111) and (200) peaks is much lower than the value reported for the conventional powder sample (1.33 versus 2.38), indicating that the diffraction from {100} planes is enhanced for the sample of Pd nanobars. It is likely that the nanobars preferentially lay on the substrate against their flat {100} facets. As a result, there was a texturing effect. The ED pattern (inset of Figure S2) taken from an assembly of Pd nanobars also indicates that they were highly crystalline. The concentric rings can be indexed to the diffraction from {111}, {200}, {220}, and {311} planes of *fcc* palladium, respectively.

Oxidative Etching and Its Role in the Anisotropic Growth of Pd Nanostructures. What is the driving force for the anisotropic growth of Pd nanobars and nanorods in the current work? Two mechanisms have been proposed to account for the anisotropic growth of a crystal in the solution phase when no template is involved. In the first mechanism, the solid materials are characterized by a highly anisotropic crystallographic structure, and they naturally grow into nanorods and nanowires. Typical examples include trigonal Se and Te, as well as würtzite CdS and CdSe.[15] The second mechanism involves twin or stacking faults, which has been observed for both 5-fold twinned nanorods and 2-fold twinned nanobeams of *fcc* metals.[16] The twin planes can generate re-entrant grooves, favorable sites for the addition of atoms.[16c] The absence of an anisotropic crystal structure or twin defects in both Pd nanobars and nanorods led us to propose a third mechanism, in which localized oxidative etching plays the pivotal role to induce anisotropic growth in a short period of time.

Oxidative etching has been extensively explored by our group and others for the shape-controlled synthesis of metal nanostructures. It can be used to slow a reduction process, selectively remove multiply twinned seeds, generate hollow Pd nanostructures, or shorten single-crystal Au nanorods.[9,10,17] Yet it can play another role in the formation of highly anisotropic nanostructures. In the present synthesis, addition of bromide at a sufficiently high concentration could cover the surface of a Pd nanocrystal with bromide due to its strong binding to the Pd surface.[18] The chemisorbed bromide layer prevents further addition of Pd atoms from solution to the nanocrystal surface, so one has to activate the surface of this nanocrystal to continue the growth. Oxidative etching, which is caused by oxygen (from air) and chloride (from $PdCl_4^{2-}$), could remove some of the bromide from the surface and thus expose sites for addition of Pd atoms. In the current case, the bromide layer would make it difficult to perform oxidative etching over the entire surface. However, with the assistance of water, oxidative etching was able to occur locally on a specific face of a cubic nanocrystal.[19] We have previously observed that corrosion of Pd nanocubes, whose surface was protected by a high concentration of PVP, occurs from only one side by a pitting process, even though all sides are equivalent {100} facets.[17b] In the galvanic replacement between Ag nanocubes and $HAuCl_4$ in water, it was also observed that etched pits were only formed at one of the six {100} faces.[20] Other groups have also reported that oxidative etching can selectively take place on {100} tips of single-crystal Au nanorods, although there are other {100} faces on the side surface.[17c] This localized oxidative etching makes one face become more active than others and thus provides favorable sites for the addition of Pd atoms. When sufficient Pd atoms are added to the etched sites, atomic addition will be faster than the dissolution of atoms caused by etching. We believe that it is the preferential growth at these active sites that breaks the cubic symmetry of a Pd nanocrystal and leads to the formation of Pd nanorods and nanobars.

This argument is supported by the experiments with different degrees of etching. Figure 3A shows a TEM image of the product obtained from a synthesis that was protected by continuous Ar flow. The resultant nanorods exhibited a decrease in aspect ratio as compared to the product prepared in air because oxidative etching was partially blocked due to the reduced level of air in the solution. However, because oxygen binds strongly to Pd surface, it is impossible to completely block oxidative etching in a Pd synthesis by simply bubbling an inert gas through the reaction solution. Most recently, we demonstrated that addition of citric acid was able to efficiently block oxidative etching.[21] Following this strategy, we added citric acid to the current synthesis, and the product was found to contain

(15) (a) Peng, X.; Manna, L.; Yang, W.; Wickham, J.; Scher, E.; Kadavanich, A.; Alivisatos, A. P. *Nature* **2000**, *404*, 59. (b) Peng, X. *Chem.-Eur. J.* **2002**, *8*, 334. (c) Xia, Y.; Yang, P.; Sun, Y.; Wu, Y.; Mayers, B.; Gates, B.; Yin, Y.; Kim, F.; Yan, H. *Adv. Mater.* **2003**, *15*, 353. (d) Peng, X. *Adv. Mater.* **2003**, *15*, 459.

(16) (a) Germain, V.; Li, J.; Ingert, D.; Wang, Z. L.; Pileni, M. P. *J. Phys. Chem. B* **2003**, *107*, 8717. (b) Sun, Y.; Mayers, B.; Herricks, T.; Xia, Y. *Nano Lett.* **2003**, *3*, 955. (c) Lofton, C.; Sigmund, W. *Adv. Funct. Mater.* **2005**, *15*, 1197. (d) Wiley, B. J.; Wang, Z.; Wei, J.; Yin, Y.; Cobden, D. H.; Xia, Y. *Nano Lett.* **2006**, *6*, 2273. (e) Elechiguerra, J. L.; Reyes-Gasga, J.; Yacaman, M. J. *J. Mater. Chem.* **2006**, *16*, 3906.

(17) (a) Xiong, Y.; Chen, J.; Wiley, B.; Xia, Y.; Yin, Y.; Li, Z.-Y. *Nano Lett.* **2005**, *5*, 1237. (b) Xiong, Y.; Wiley, B.; Chen, J.; Li, Z.-Y.; Yin, Y.; Xia, Y. *Angew. Chem., Int. Ed.* **2005**, *44*, 7913. (c) Tsung, C.-K.; Kou, X.; Shi, Q.; Zhang, J.; Yeung, M. H.; Wang, J.; Stucky, G. D. *J. Am. Chem. Soc.* **2006**, *128*, 5352.

(18) (a) Schimpf, J. A.; Abreu, J. B.; Soriaga, M. P. *J. Electroanal. Chem.* **1994**, *364*, 247. (b) Carrasquillo, A.; Jeng, J.-J., Jr.; Barriga, R. J.; Temesghen, W. F.; Soriaga, M. P. *Inorg. Chim. Acta* **1997**, *255*, 249. (c) Lucas, C. A.; Marković, N. M.; Ross, P. N. *Phys. Rev. B* **1997**, *55*, 7964. (d) Zou, S.; Gao, X.; Weaver, M. J. *Surf. Sci.* **2000**, *452*, 44.

(19) (a) Newman, R. C.; Sieradzki, K. *Science* **1994**, *263*, 1708. (b) Scully, J. C. *The Fundamentals of Corrosion*, 3rd ed.; Pergamon Press: Oxford, New York, 1990; pp 1−57.

(20) Sun, Y.; Xia, Y. *J. Am. Chem. Soc.* **2004**, *126*, 3892.

(21) Xiong, Y.; McLellan, J. M.; Yin, Y.; Xia, Y. *Angew. Chem., Int. Ed.* **2007**, *46*, 790.

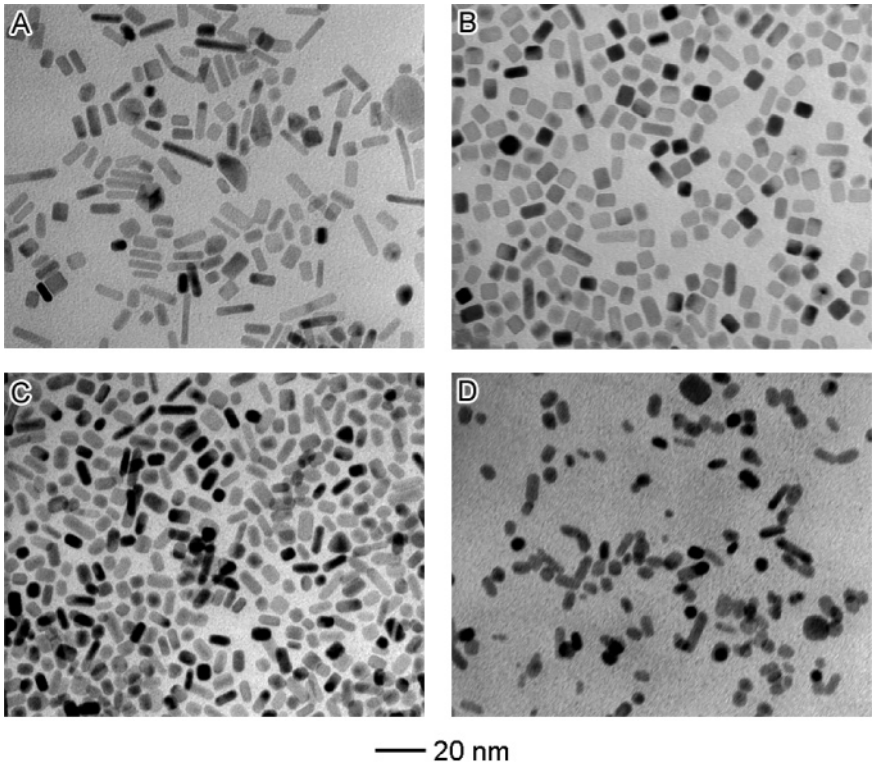

Figure 3. TEM images of Pd nanostructures synthesized when oxidative etching was retarded (A) by bubbling with Ar gas and (B) in the presence of 0.13 M citric acid; or enhanced (C) in the presence of 0.20 M NaCl and (D) 1 M HCl. All of the syntheses were carried out under the same condition as in Figure 1D, except for the difference noted above.

nanocubes and short nanobars instead of nanorods (see Figure 3B). This observation indicates that the lack of oxidative etching inhibited the anisotropic growth of nanocrystals. On the other extreme, when oxidative etching was enhanced, etching would take place over the entire surface of each particle rather than locally on a specific face, in a way to eliminate the difference between different faces. When NaCl was added to the reaction system to enhance oxidative etching, we observed a decrease in aspect ratio for the nanostructures as shown in Figure 3C. The oxidative etching could be further enhanced by adding HCl instead of NaCl.[10] Figure 3D shows a typical TEM image of the sample prepared with the use of HCl. The aspect ratio of Pd nanostructures was further reduced to 1−3, as compared to Figures 1D and 3C. From these results, it can be concluded that localized oxidative etching is responsible for the anisotropic growth of Pd nanobars and nanorods.

Adsorption of Bromide on the Surface of Pd Nanostructures. In the present synthesis, bromide played a critical role in the formation of nanostructures enclosed by the {100} and {110} side facets. According to the Wulff construction, the thermodynamically favored shape of an *fcc* metal is cuboctahedron under the vacuum condition.[8,9] In a solution-phase process, impurities or capping agents can alter the surface free energies via adsorption and thus induce new shapes.[8c] For instance, the {100} facets of an *fcc* metal can be stabilized through chemical interactions with the oxygen and/or nitrogen atoms of the pyrrolidone units of PVP, leading to the formation of truncated Pd nanocubes >25 nm in size.[16b,17a] However, a polymer is too big to have a capping effect on smaller nanocrystals. As a result, the PVP-stabilized Pd nanoparticles <10 nm in size usually have a cubooctahedral shape.[9] When bromide was introduced into the reaction system, it is able to chemisorb onto the surface of Pd seeds and alters the order of surface free energies.[18] This modification to surface energy also plays an important role in facilitating the formation of anisotropic Pd nanostructures such as nanobars and nanorods that are enclosed by {100} and {110) side facets.

To decipher the role of bromide, we performed a series of syntheses by altering the concentration of KBr in the synthesis, and the results are summarized in Figure 4. As expected, synthesis in the absence of bromide only produced cuboctahedrons. Addition of bromide gradually alters the shape of products to nanobars and nanorods. The appearance of these new shapes implies that the presence of bromide can promote the formation of {100} and {110} facets. The concentration of bromide is also critical to the control of product shape. At low concentration of bromide, the product was a mixture of both nanobars and nanorods (see Figure 4B). When the molar ratio of KBr to Na_2PdCl_4 was increased from 8 through 15 to 30, the major product became nanorods (Figures 4B,C and 1D). Further increase of bromide concentration led to a decrease for the aspect ratio, as shown in Figure 4D. This dependence of morphology on the concentration of bromide can be understood by the following argument: when the concentration of bromide was increased, the coverage of bromide on particle surface also increased. A higher coverage would protect the nanocrystals better from oxidative etching, and thus make the reaction faster, favoring the formation of nanorods. Because oxidative etching is the key to the formation of nanorods, lack of etching in the reaction system would also restrain their anisotropic growth, resulting in a decrease of the aspect ratio.

It is worth pointing out that the major function of bromide in the current synthesis is its chemisorption on nanocrystal surface. As bromide is less corrosive than chloride, it cannot

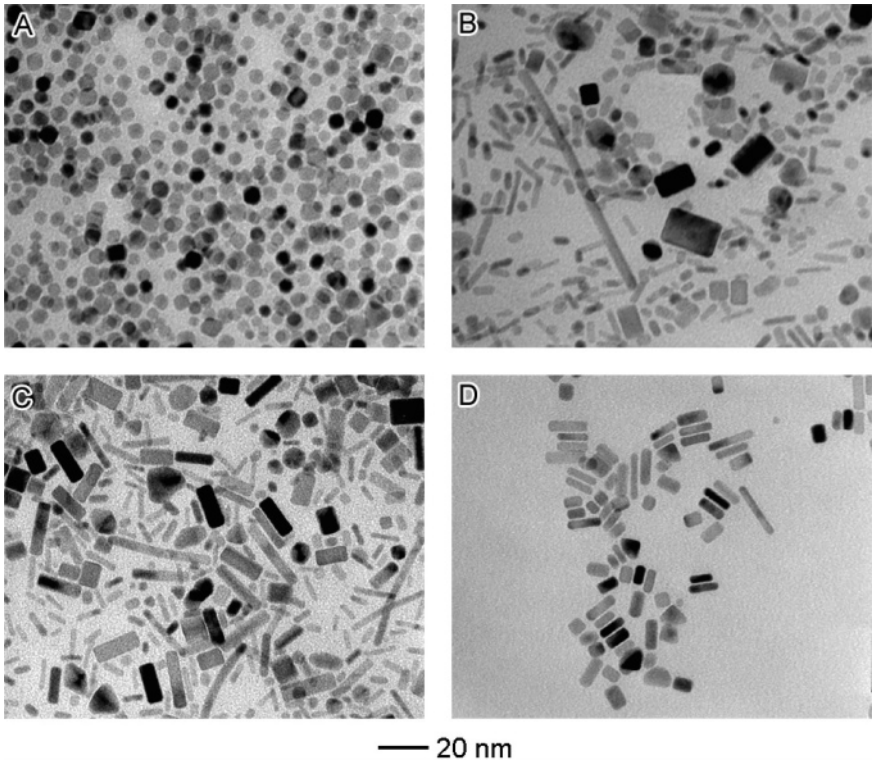

Figure 4. TEM images of Pd nanostructures synthesized in the presence of KBr at different concentrations, demonstrating the role of bromide in promoting {100} and {110} surfaces. The molar ratio of KBr to Na_2PdCl_4 was: (A) 0; (B) 8; (C) 15; and (D) 50. All of the syntheses were carried out under the same condition as in Figure 1D, except the variation of KBr concentration.

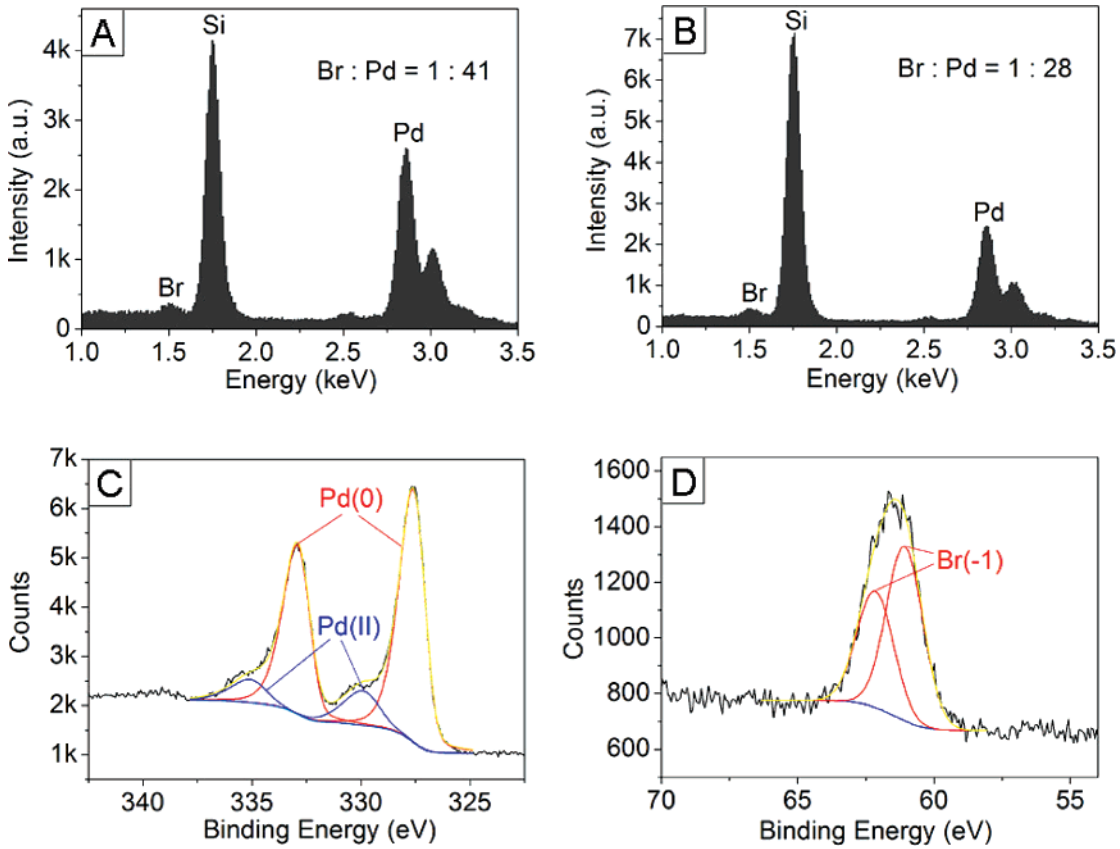

Figure 5. (A,B) EDX spectra taken from the nanobars shown in Figure 1B: (A) as-synthesized and (B) after extensive washing with water. (C) High-resolution Pd 3d XPS core level spectrum taken from the nanobars. (D) High-resolution Br 3d XPS core level spectrum recorded from the nanobars. The nanobars were extensively washed with water before XPS measurements.

make a major contribution to the oxidative etching. For example, when Na_2PdBr_4 instead of Na_2PdCl_4 was used as the precursor, the morphology exhibited a similar dependence on the concentration of bromide, as shown in Figure S3. As compared to the

case with Na_2PdCl_4, the samples prepared with Na_2PdBr_4 displayed lower aspect ratios. This difference can be attributed to the fact that the rate of oxidative etching was reduced in the absence of chloride (from the Na_2PdCl_4 precursor).

The presence of bromide on the surface of Pd nanostructures was further confirmed by EDX analysis. Figure 5A and B shows EDX spectra taken from Pd nanobars without washing and after extensive washing with deionized water, respectively. The presence of bromine signals after extensive washing implies that there is a high concentration of bromide strongly bonded to the particle surface. The binding energies of Pd and Br were examined by XPS analysis. The depth of XPS penetration is about 6−10 nm, which ensures the detection of all of the atoms on or in each nanobar. Figure 5C shows the Pd 3d core level spectrum, which includes two sets of 3d peaks. One set shows Pd $3d_{5/2}$ and Pd $3d_{3/2}$ at 335.2 and 340.5 eV, respectively, which are in accordance with the literature values for bulk Pd(0).[22] The other set includes a Pd $3d_{5/2}$ peak at 337.5 eV and a Pd $3d_{3/2}$ peak at 342.6 eV, which are close to the reported values for Pd(II)-type samples such as $PdBr_2$.[22] The ratio of Pd(0) to Pd(II) is about 5.27. As shown by the XRD and ED patterns in Figure S2, there should be no $PdBr_2$, PdO, or other impurities in the sample. A percentage of Pd(II) as high as 16% suggests that Pd atoms on the surface donated electrons to Br for chemical bonding. The Br $3d_{5/2}$ and Br $3d_{3/2}$ binding energies are determined to be 68.7 and 69.8 eV, respectively (see Figure 5D), which were very close to the literature values for KBr (68.5 and 69.6 eV).[22] As compared to the spectrum of KBr (Figure S4), the Br 3d peaks in Figure 5D are much broader. The broadening and small shift of the Br 3d peaks could be attributed to the binding of Br to Pd surface.

The selection of an appropriate anion for chemisorption is also instrumental in the growth of Pd nanocrystals with anisotropic shapes. As reported in literature, the strength of chemisorption or surface coordination to Pd surface increases in the order of chloride < bromide < iodide.[18b] For this reason, when KCl was used instead of KBr, the surface protection and promotion of {100} and {110} surfaces were not remarkable, and the product mainly consisted of cuboctahedrons (Figure 6A). On the contrary, the chemisorption of iodide on the nanocrystal surface is so strong that the particles are difficult to grow into larger sizes with a well-defined shape (Figure 6B).

Controlling the Shape of Pd Nanostructures. Kinetic control has been used to synthesize metal nanostructures with a number of different shapes. For example, we and other groups have prepared nanoplates of Ag, Au, and Pd by slowing the reduction kinetics.[10,12] The slow reduction can induce the formation of stacking faults and thus break the cubic symmetry.[16] However, over 70% of the surface of these nanostructures were covered by the {111} facets. In the current system, a different mechanism seems to be involved, although it also involves manipulation of reduction and growth kinetics. Based on the results presented in the previous sections, it is not difficult to recognize that three key factors are responsible for the formation of Pd nanostructures enclosed by {100} and {110} facets: bromide adsorption, oxidative etching, and reduction kinetics. In the presence of surface adsorption and localized oxidative etching, the rates of nucleation and atomic addition to the surface of seeds (i.e., growth) can be manipulated by controlling the reduction kinetics to generate well-defined nanostructures such as nanobars and nanorods with different aspect ratios.

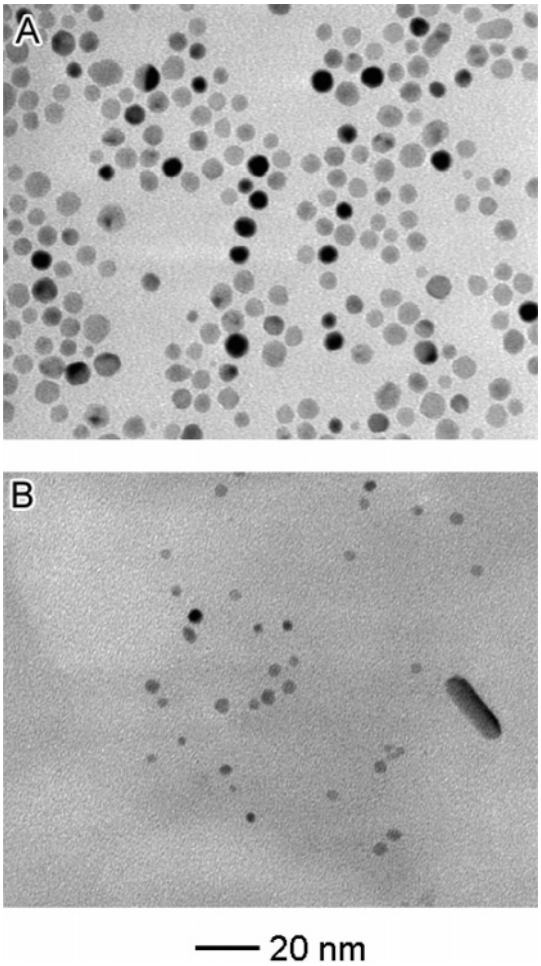

Figure 6. TEM images of Pd nanoparticles synthesized by using KCl or KI instead of KBr: (A) KCl and (B) KI. All of the syntheses were carried out under the same condition as in Figure 1D, except for the substitution of KBr by KCl or KI at the same molar concentration.

As shown in the schematic illustration (Figure 7A), the adsorption of bromide can alter the order of surface free energies, and slightly truncated nanocubes rather than cuboctahedrons will become the most favorable shape. When the reduction rate is in the low or medium regions, the seeds take a cubic shape with slight truncation at the corners. Although the *fcc* lattice of Pd is highly symmetric, localized oxidative etching creates an active site on one of the six faces, for example, the (100) face, for atomic addition and facilitates the preferential growth along the *a*-axis in a short period. This preference will break the symmetry of an *fcc* structure and lead to the formation of nanobars. At a low rate of atomic addition, the rate of growth along the *a*-axis is not much higher than that of etching on the (100) face, so that the effect of preferential growth along the *a*-axis is not distinct and thus the aspect ratios of the resultant nanobars are very small (1−1.2). When atomic addition is fast enough, preferential growth on the (100) face becomes most favorable, leading to the formation of nanobars with higher aspect ratios.

(22) (a) Kumar, G.; Blackburn, J. R.; Jones, M. M.; Albridge, R. G.; Moddeman, W. E. *Inorg. Chem.* **1972**, *11*, 296. (b) Rochefort, A.; Bertolini, J. C.; Abon, M.; Delichere, P. *Surf. Sci.* **1993**, *294*, 43. (c) Briggs, D.; Seah, M. P. *Practical Surface Analysis*; John Wiley & Sons: New York, 1993; Vol. 1.

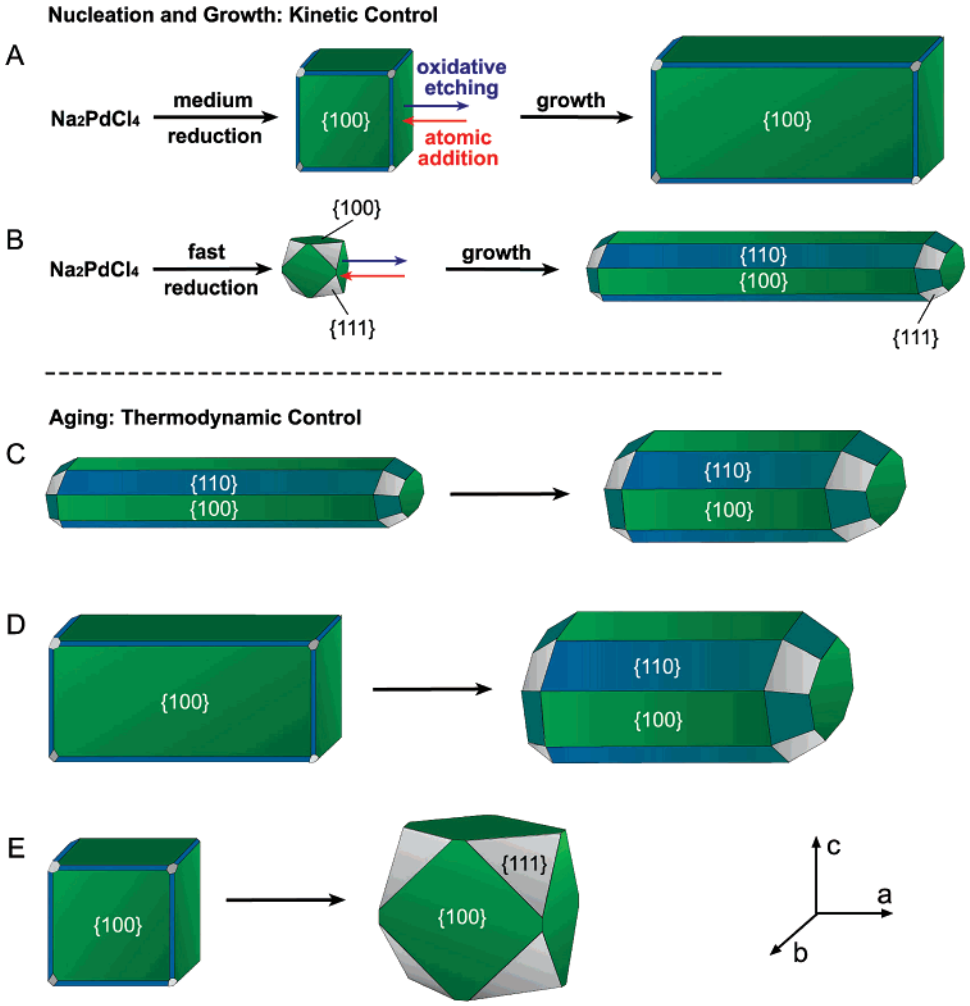

Figure 7. Schematic illustration of the mechanisms responsible for the formation of nanobars and nanorods, as well as the morphological changes in an aging process: (A) nucleation and formation of nanobars at a medium reduction rate; (B) nucleation and formation of nanorods at a fast reduction rate; (C) decrease of aspect ratio for nanorods; (D) evolution of nanobars into nanorods; and (E) evolution of nanobars with an aspect ratio of ~1 (i.e., nanocubes) into cuboctahedrons.

As the reduction rate becomes much faster, the synthesis will follow a different path. Under this condition, more seeds will be formed in the nucleation stage. At the same concentration of Pd precursor, an increase in the number of seeds results in the production of nanocrystals with smaller sizes. On the other hand, the fast nucleation makes the cubic seeds have more significant truncation at the corners, with a shape more close to cuboctahedron. As illustrated in Figure 7B, preferential growth of a cubooctahedral seed along the *a*-axis will induce {110} facets as well as {100} facets to be the side surface. The appearance of {110} facets as the side faces will result in the rod-shaped nanostructures with an octagonal cross-section. As a result, the final product is dominated by nanorods thinner than the nanobars. This mechanism can also explain why the shape of the final product can be tailored by manipulating the reduction kinetics.

Formation of Au Nanorods and Pt Nanobars. We have also applied the same strategy to the synthesis of single-crystal Au nanorods. Figure 8A shows a typical TEM image of Au nanorods synthesized in the presence of KBr. The nanorods have a diameter of ca. 2.5 nm and length up to 20 nm. The yield of nanorods was around 40%, while the other 60% of the product was microscale aggregates. Such Au nanorods have been intensively studied by several groups, and here we note that their structure is the same as that of the Pd nanorods with the side faces being bounded by a mix of {100} and {110} facets.[8,11] Murphy and co-workers have also noticed that the bromide in the surfactant hexahecyltrimethylammonium bromide (CTAB) might play an important role in the formation of Au nanorods.[23] The bromide was thought to adsorb onto the side faces of Au seeds and then confine the lateral growth of nanorods by recruiting the cationic surfactant to form a bilayer. The long surfactant tails were proposed as a major driving force for the anisotropic growth. In addition, a small amount of Ag cations must be added to induce the formation of single-crystal Au nanorods in their work. Here, we found that the bromide alone could also alter the surface energies and promote highly anisotropic growth. This unique feature of bromide will certainly attract the attention of the research community, and it is anticipated that it will serve as a new knob for controlling the shape of metal nanostructures. Note that the size of our Au

(23) (a) Gao, J.; Bender, C. M.; Murphy, C. J. *Langmuir* **2003**, *19*, 9065. (b) Murphy, C. J.; Sau, T. K.; Gole, A. M.; Orendorff, C. J.; Gao, J.; Gou, L.; Hunyadi, S. E.; Li, T. *J. Phys. Chem. B* **2005**, *109*, 13857. (c) Murphy, C. J.; Gole, A. M.; Hunyadi, S. E.; Orendorff, C. J. *Inorg. Chem.* **2006**, *45*, 7544.

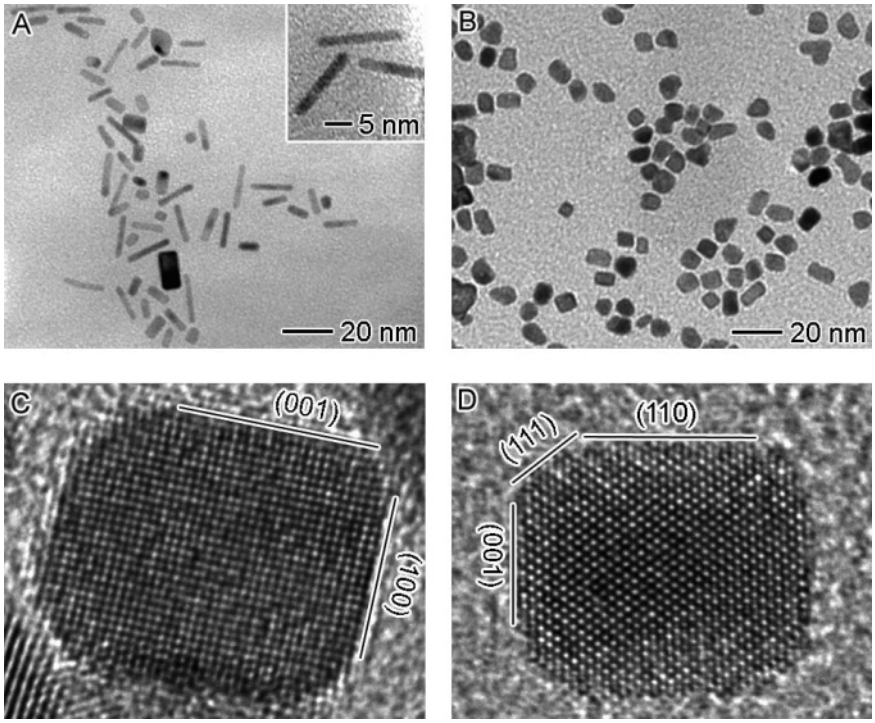

Figure 8. TEM images of Au nanorods and Pt nanobars synthesized using a similar approach: (A) Au nanorods (with the inset showing a blow-up image), and (B) Pt nanobars. (C,D) High-resolution TEM images of (C) a Pt nanobar recorded along [010] and (D) a Pt nanobar recorded along [1$\bar{1}$0]. The syntheses were performed with a molar ratio of KBr to $HAuCl_4$ (or Na_2PtCl_6) at 30, in the presence of 75 mM PVP, and in an 11-mL mixture of EG (72.7%) and water at 140 °C.

nanorods is much smaller as compared to that of the Au nanorods made by the Murphy group (3 nm vs 15−30 nm in thickness).

This method can also be extended to Pt. As shown in Figure 8B, the product consisted of nanobars with an aspect ratio of 2−3 and a yield above 90%. Figure 8C shows a high-resolution TEM image of a Pt nanobar recorded along [010]. The fringes show a period of 1.9 Å, which was consistent with the {200} lattice spacing of *fcc* Pt. This image also displayed well-resolved, continuous fringes with the same orientation, suggesting that each Pt nanobar is a piece of single crystal enclosed by {100} facets. Figure 8D shows a high-resolution TEM image of a Pt nanobar with a different structure, which was recorded along [1$\bar{1}$0]. The side facets are {110}, and the growth direction is also [001]. The ends of the nanobar are terminated by the (001) face and {111} facets. These two types of 1-D structures are different from the Pt nanorods and nanowires growing along the [111] axis that were prepared using the iron-mediated polyol process.[24] This result also supports the argument that addition of bromide favored the formation of {100} and {110} surfaces.

Stability of the Pd Nanostructures. As discussed above, the formation of Pd nanobars and nanorods was governed by kinetics. For this reason, they are not thermodynamically stable due to their relatively high surface energies. To evaluate their stability, the products were aged in the reaction solution for 2 weeks at room temperature. As shown in Figure 9A, the diameter of nanorods increased while their length decreased during the aging process. For the nanobars, the aging process made them more severely truncated (see Figure 9B). High-resolution TEM images (Figure 9C) indicate that the nanobars had been evolved into nanorods with both {110} and {100} facets as side faces. The high-resolution TEM study also revealed that the nanobars with an aspect ratio of ~1 transformed into cuboctahedrons, a shape more favored by thermodynamics, as depicted in Figures 9D and S6. The short nanorods formed through the aging process should be some intermediates on the pathway to the thermodynamically favorable shape.

These observations imply that the anisotropic nanostructures formed through kinetic control were not stable shapes and they would evolve into the thermodynamically favorable shape. This aging process is supposed to be mainly governed by thermodynamics, following a process illustrated in Figure 7C−E. The loss of atoms from {111} facets and the addition of atoms to {100} facets resulted in the enlargement of {111} facets and the shrinkage of {100} facets, transforming Pd cubes into cuboctahedrons (see Figure 7E). Multiple processes might be involved in this shape evolution, such as oxidative etching, desorption of bromide, and surface diffusion. However, minimization of the surface energy of a particle should be the major driving force for such a transformation.

It is worth pointing out that the Pd nanorods in Figure 1 should be formed via growth from small, near spherical seeds, rather than through the evolution of nanobars in an aging process. This point was supported by the evolution of shape, which was monitored with TEM by taking samples at various reaction times (Figure S7). The TEM observation suggests that the Pd nanorods could be formed in the stage as early as t = 10 min. The smaller diameter of nanorods relative to nanobars (2 vs 6 nm, Figure 1) also supports this argument because nanorods evolved from nanobars during aging should have a thicker diameter.

(24) (a) Chen, J.; Herricks, T.; Geissler, M.; Xia, Y. *J. Am. Chem. Soc.* **2004**, *126*, 10854. (b) Teng, X.; Yang, H. *Nano Lett.* **2005**, *5*, 885. (c) Song, H.; Kim, F.; Connor, S.; Yang, P. *J. Phys. Chem. B* **2005**, *109*, 188.

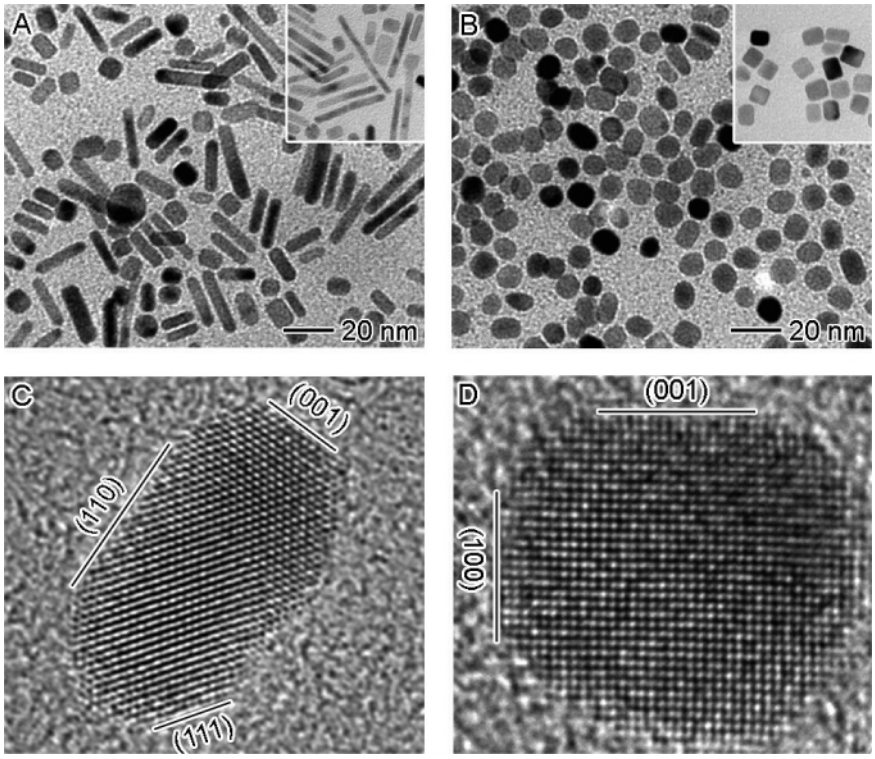

Figure 9. Electron microscopy characterization after the Pd nanorods and nanobars in Figure 1F and A had been aged in the reaction solution for 2 weeks at room temperature: (A) TEM image of nanorods after aging; (B) TEM image of nanobars after aging; (C) high-resolution TEM image of a nanobar with an aspect ratio of ~2.5 after aging that was recorded along [110]; and (D) high-resolution TEM image of a nanobar with an aspect ratio of ~1 after aging that was recorded along [010]. The insets in panels (A) and (B) show two TEM images of the corresponding samples before the aging process, at the same magnification as in (A) and (B).

4. Conclusion

We have demonstrated a new strategy for growing highly anisotropic nanostructures of Pd, single-crystal nanobars bounded by {100} facets and single-crystal nanorods with their side surfaces enclosed by {100} and {110} facets. According to both the theoretical prediction and the experimental observation, Pd atoms should nucleate and grow in a solution phase to form the thermodynamically favored shape, cuboctahedrons with the surface bounded by a mix of both {111} and {100} facets.[9,10] In the current work, we combined the following three processes to obtain elongated nanostructures: (i) speedy reduction of precursor to ensure prompt addition of atoms to the seed; (ii) chemisorption of bromide on the seed surface to alter the order of free energies of different facets and promote the formation of {100} and {110} facets; and (iii) localized oxidative etching on one specific face of the seed to break the cubic symmetry. The involvement of bromide absorption was confirmed by XPS and EDX analyses on the products. These anisotropic nanostructures formed via kinetic control were not stable, and they tended to evolve into the thermodynamically favored shape during aging.

This work demonstrates, for the first time, that cubic symmetry of an *fcc* metal can not only be broken by forming twin defects but also through localized oxidative etching. Note that the localized oxidative etching is usually caused by a trace amount of oxygen, chloride, and water, which could originate from a minor change in experimental parameters such as the source of chemical reagents and the choice of glassware. These results emphasize again the importance and necessity to precisely control the experimental parameters in a solution-phase synthesis. This work also suggests the role of bromide as a capping agent to influence the surface energies of different facets of an *fcc* metal and therefore induce the formation of new shapes not favorable from the perspective of thermodynamics. Certainly, a more direct contribution of this work to the chemistry community is the demonstration of a simple and versatile method for growing highly anisotropic, single-crystal nanostructures of noble metals, including Pd, Au, and Pt. Although modification to the experimental procedures might be required, it is expected that this generic method could be further extended to grow longer Pd nanowires that will find immediate use in the fabrication of electronic and sensing devices.

Acknowledgment. This work was supported in part by the ACS (PRF-44353-AC10) and NSF (DMR-0451788), as well as a fellowship from the David and Lucile Packard Foundation. X.Y. is a Camille Dreyfus Teacher Scholar (2002−2007). J.W. has been supported by a grant from CNMT-MOST (No. M105KO010026-05K1501-02611). We are grateful to Dr. Lara Gamble for her assistance with XPS analysis. This work used the Nanotech User Facility (NTUF), a member of the National Nanotechnology Infrastructure Network (NNIN) funded by the NSF.

Supporting Information Available: Filtered high-resolution TEM images of the nanobars and nanorods of Pd and Pt; PXRD and ED patterns of Pd nanobars; and TEM images of Pd nanoparticles synthesized with Na_2PdBr_4 as the precursor. This material is available free of charge via the Internet at http://pubs.acs.org.

JA0688023